Supplementary Information

(Dated: January 15, 2015)

I. MOVIES

Movie 1:- A fruit fly undergoing a typical roll perturbation and correction maneuver, corresponding to the same data shown in Figure 2. The three sides of of the 3D box show the raw movies from the three fast cameras. The 3D-rendered fly represents the kinematic data of the body and wing positions in each frame. The fly's center-of-mass trajectory is shown by a green line, on which the red segment corresponds to the location of the perturbation. The time in ms is shown on the bottom left corner. The movie is played three times to show the same maneuver from different views. The third time also shows traces of the wing-tip positions.

Movie 2:- Roll perturbation and correction maneuver during nearly-hovering flight. The fly was perturbed 35° to its right and corrected to 10% of the perturbation within $T_c = 25$ms, or 5.5 wing-beats. Full correction $\rho = 0$ was obtained at $t = 28$ms. By 40ms the fly shows a slight over-correction to $\rho = -5°$. The yaw deflection that accompanied the roll perturbation is also seen.

Movie 3:- Roll perturbation and correction maneuver in which the perturbation was applied when the fly was already rolled by 20° to the right. Prior to the perturbation the fly was also flying with apparent side-slip. The fly corrected to zero roll 30ms after the onset of the perturbation. A yaw-right deflection as a result of the external torque is evident.

Movie 4:- Roll correction maneuver following two consecutive perturbation pulses. When the movie starts the fly is already correcting for the first pulse. The second pulse is applied at $t = 0$ for 5ms. The leg-spreading response as a result of the first pulse is clearly seen. This correction maneuver is indistinguishable from maneuvers following single-perturbation pulses, in terms of the body and wing kinematics as well as the parameters of the PI controller. The corresponding data is shown in Figures S2 and S3.

Movie 5:- Extreme roll perturbation event, corresponding to Fig. 7. The fly was rolled 8 full times to its right by a series of magnetic pulses. The fly regained control $3-4$ wing-beats after the perturbation ended. Full correction to $\rho = 0$ was not captured in the movie since the fly exited the filming volume. Note that during the perturbation the fly was unable to oppose the magnetic torque. In fact, the right wing, which in a typical correction maneuver should have been flapping with a larger stroke amplitude, hardly flapped at all and occasionally even seemed disconnected from its flight power muscles.

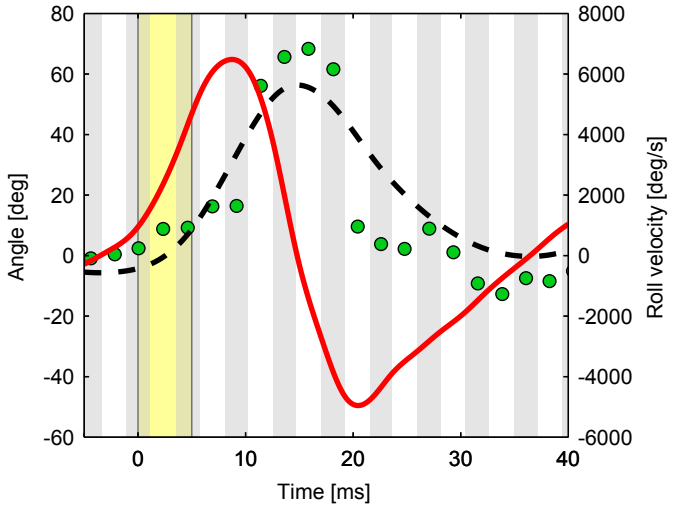

FIG. S.1. The roll angle (black dashed line), roll velocity (solid red line) and the fly's response $\Delta\Phi$ (green circles) as a function of time, for the correction maneuver in Figures 1 and 2 in the main text. The vertical gray stripes indicate back strokes and the white stripes indicate forward strokes. Note the two vertical axis measuring angle (for ρ and $\Delta\Phi$) and angular velocity (for $\dot{\rho}$).

II. ROLL AND $\Delta\Phi$ KINEMATICS

Figure S.1 shows the roll angle (dashed), roll velocity (red) and the fly's response $\Delta\Phi$ (green circles) as a function of time, for the correction maneuver in Figures 1 and 2 in the main text. The fly's response is almost instantaneous with the roll kinematics, supporting our result that an I-only control model, in which $\Delta\Phi \propto \rho$, must have an unfeasibly small response time. The roll velocity rises and peaks before the roll angle, thus a PI control model that includes the roll velocity follow the changes in the roll angle despite its latency.

III. CONTROL MODEL FITTING

To fit the parameters of the PI control model $\Delta\Phi_{\mathrm{model}}$ (Eq. 3) to the measured data we define the following error function:

$$E(\Delta T, K_{\rm p}, K_{\rm i}) = \frac{1}{N}\sum_{j=1}^{N}\big[\Delta\Phi_{\rm model}(\Delta T, K_{\rm p}, K_{\rm i}, t_j) - \Delta\Phi_{\rm expr}(t_j)\big]^2, \quad \text{(S.1)}$$

whose minimization gives the three fitted parameters. The discrete times t_j are the mid-halfstroke times when $\Delta\Phi_{\rm expr}(t_j)$ was measured (green circles in Figs. 2, S.4f). The fit process considered data measured between $t = \Delta T$ and $t = 40$ms, to include only the correction maneuver. Because $E(\Delta T, K_{\rm p}, K_{\rm i})$ is fast to calculate and the range of each of its parameter could be readily confined, we were able to evaluate the error function on a grid in the 3D parameter space and directly examine the structure of the error function. We could limit the range of each parameter, for example, ΔT is positive and bounded by the duration of the entire correction maneuver. The other two parameters are either zero or positive and their upper search bounds were determined based on reasonable cut offs given the trends in the errors. Hence, we could directly verify that the function has a single global minimum within the evaluated parameter range. The minimum was obtained on one of the grid points. The grid spacing was fine enough such that going to nearby points had negligible change in the cost function compared with measurement accuracy. Fig. S.2 illustrates the error landscape for the maneuver shown in Fig. 2, by plotting the contours of $E - E_{\rm min}$ in three orthogonal cross sections around the global minimum $E_{\rm min}$.

We use such plots to evaluate the confidence intervals (CI) of the fitted controller parameters. We assume that the distribution of the measurement error of $\Delta\Phi_{\rm expr}$ is Gaussian, $N(0, \sigma^2)$, with zero mean and $\sigma = 2°$. This measurement error was evaluated in a previous paper by our group [1] and also verified manually for each wing stroke in the current data set. The reduced error function is, therefore, $e = E/\sigma^2$. If the model perfectly predicted the data, the reduced error function becomes a sum of the squares of N independent standard normal random variables, namely, the χ^2 distribution. The confidence interval is obtained by evaluating the change in a parameter that results in a unity change in e or, equivalently, a σ^2 change in the error function E. In Fig. S.2 the contour of $\sigma^2 = 4$ corresponds to the estimated confidence intervals of the three fitted parameters in the specific maneuver: $\Delta T = 4.4 \pm 0.25$ms, $K_{\rm p} = 6 \pm 0.5$ms, and $K_{\rm i} = 0.7 \pm 0.05$.

IV. RECOVERY FROM A DOUBLE PULSE PERTURBATION

Figures S.3 and S.4 show measured data for a recovery maneuver from a double pulse perturbation (Movie 4). The results show the same correction mechanism as for a single pulse perturbation (Figures 1 and 2 in the main text).

V. ANALYZING PREVIOUSLY PUBLISHED DATA ON ROLL RESPONSE OF TETHERED FLIES

To further test the PI control model, we used it to predict the roll-response of tethered fruit flies previously published by Dickinson in [2]. In these tethered experiments flies were mounted on a gimbaled apparatus oscillating along a given axis, such that the flies had no visual cues relating to the imposed rotation. The wing-stroke amplitudes were measured using phorodetectors that recorded the shadow of each wing. We focus on the roll-response measurements, in which flies were oscillated along a horizontal roll axis termed "functional roll" ($h_{\rm b}$ in Fig. 1c in the main text). Although this axis is different than the Euler roll axis considered in this paper, it can be shown for a fly pitched up by 45°, a given rotation along the "functional roll" generates almost the same deflection along the Euler roll. Hence, when discussing rotations along the Euler roll angle, the two roll definitions are practically equivalent.

The stroke amplitude of the left wing was measured during an oscillating roll perturbation with an amplitude $A = 25°$, period $T = 0.63$s, and a maximum roll velocity of $250°{\rm s}^{-1}$. The roll angle is described by $\rho(t) = A\sin(\omega t)$ and the roll velocity is $\dot\rho(t) = A\omega\cos(\omega t)$. The wing response data was plotted both as a function of the roll angle (Fig. 3d, [2]) and roll velocity (Fig. 3e, [2]). We applied standard image analysis techniques to extract the data from these two plots and used the data to find the parameters of the corresponding PI controller, as described below (Figs. S.5 and S.6).

Since the roll oscillation period in the tethered experiment is 630ms, the time delay measured in the free flight experiments $\Delta T \approx 5$ms is negligible. Hence the response in the tethered experiment is effectively instantaneous and the functional form of the controller can be written as:

$$\Delta\Phi_{\rm Left}(t) = \frac{1}{2}\Big(K_{\rm p}\dot\rho(t) + K_{\rm i}\rho(t)\Big), \quad \text{(S.2)}$$

in which $\Delta\Phi_{\rm Left}(t) \equiv \Phi_{\rm Left}(t) - \Phi_{\rm Mean}$ is the deviation of the left wing amplitude from its mean value $\Phi_{\rm Mean}$. The $\frac{1}{2}$ factor is due to the fact that data was measured for the left wing rather than for the stroke amplitude difference between the wings (as in Eq. 3 in the main text). Twice the slope of the linear fit to $\Phi_{\rm Left}(\dot\rho)$ reported in [2] was used to obtain $K_{\rm p} = 32.2$ms. To obtain $K_{\rm i}$ we manually fit the data and obtain a value of $K_{\rm i} = 0.2$. A fitting algorithm was not used for $K_{\rm i}$, because many data points were clustered near $\pm 25°$ and could not be extracted.

The prediction of the PI controller fit are plotted in Figs. S.5 and S.6 along with the extracted data from [2]. Fig. S.5a shows that the prediction of the PI model plotted as a function of the roll angle yields an ellipse with $R^2 = 0.77$. Similarly, the PI model prediction as a function of the roll velocity (Fig. S.5b) also yields an ellipse

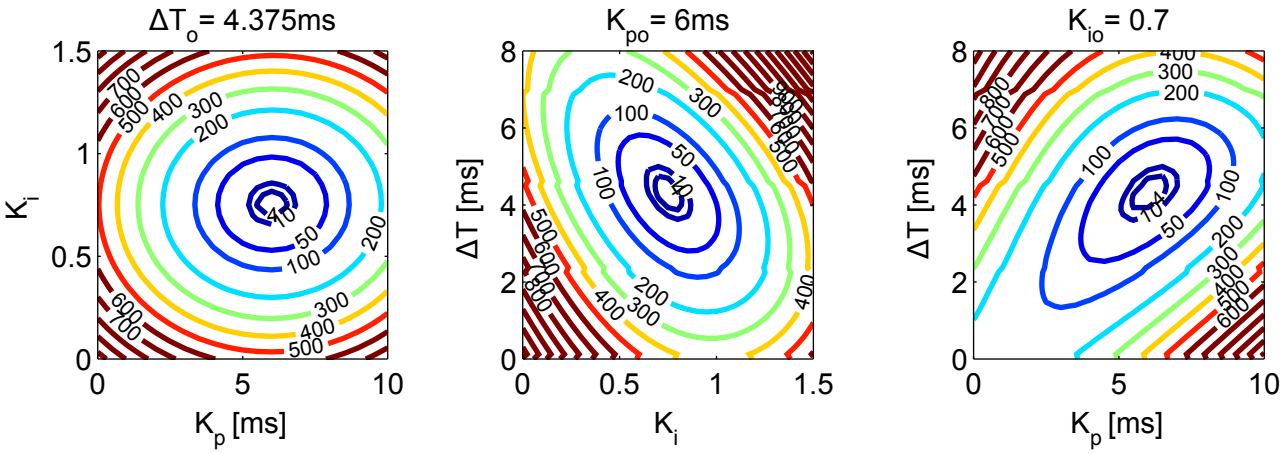

FIG. S.2. The error landscape for the fitting process of a PI controller model for the movie shown in Figs. 1 and 2 of the main text. The three panels show contours of the error function $E(\Delta T, K_\mathrm{p}, K_\mathrm{i})$ in three orthogonal cross section that coincide at the minimum of E. The numerical values of the minimizing parameters $(\Delta T_\mathrm{o}, K_\mathrm{po}, K_\mathrm{io})$ are given in the title of each panel. The inner-most counter of $\sigma^2 = 4$ corresponds to the evaluated confidence interval.

with $R^2 = 0.82$ (compared with $R^2 = 0.62$ of the linear fit). The measured data and PI-model prediction are also plotted in the 3D space whose axes are $(\rho,\ \dot\rho,\ \Phi_\mathrm{Left})$ (Fig. S.6). We find that the Φ_Left output as a function of the $(\rho,\ \dot\rho)$ stimulus is well described by an inclined ellipse.

The 3D shape of the response Φ_Left as a function of $(\rho,\ \dot\rho)$ lies on a plane defined by (Eq. S.2). In this particular case, the stimulus is sinusoidal in time so that in the $(\rho,\ \dot\rho)$ plane it forms an ellipse. The corresponding response is an inclined ellipse that lies on the response plane. Hence, plotting the projections of the 3D ellipse, as in the plots of $\Phi_\mathrm{Left}(\rho)$ and $\Phi_\mathrm{Left}(\dot\rho)$ in [2], each yield an ellipse (Fig.S.5a,b).

Intuitively, the upper right quadrant of the ellipse in Fig.S.5a corresponds to times when the fly is rolled to its left ($\rho > 0$) with a leftward roll velocity ($\dot\rho > 0$). The response is maximum at these times because the two terms of the PI controller are positive (Eq. S.2). The bottom right quadrant of the ellipse in Fig.S.5a corresponds to times when the fly is rolled to its left ($\rho > 0$) but with a rightward roll velocity ($\dot\rho < 0$). The response at these times is smaller than at the upper left quadrant since the two terms in Eq. S.2 have opposite signs. Similarly, the response is minimum when $\rho < 0$ and $\dot\rho < 0$ (bottom left quadrant).

Finally, following [2], we plot the fly's response as a function of the roll acceleration (Fig. S.7), along with the prediction of the PI control model. Note, that the PI model is a function of roll angle and roll velocity, and does not use information about roll acceleration. Still, the plot shows that the PI model can explain the observed behavior without using the roll acceleration. It supports the hypothesis that fruit flies do not measure their roll acceleration.

The prediction of the PI controller model is also consistent with measurement of the temporal response of a fly to a roll perturbation (Fig. 2 in [2]). The tethered experiment showed a mean stroke amplitude difference between the two wings of $\Delta\Phi = 8°$ (peak-to-peak) in response to an sinusoidal roll stimulus of 25° amplitude and 0.8s period. Using the PI controller (Eq. 3 in the main text) with the parameters fitted above predicts a response of $\Delta\Phi = 8.0°$. Moreover, the phase of the response with respect to the stimulus is also predicted by the model. The peak asymmetry was observed at times between the maxima of ρ and the maxima of $\dot\rho$, implying that both terms of Eq. S.2 have comparable contributions to the response, as we see in the free flight experiments.

The values of the controller parameters fitted for the tethered experiment are different than the controller parameters fitted to the free flight experiment reported here (Table II). Possible reasons for this difference are natural variablity among flies (as characterized by the free flight data) as well as the different experimental methods: using tethered compared to free flying animals.

In summary, the PI controller well-describes results of previous experiments with tethered flies, with a correlation coefficient between the predicted and measured wing amplitude of 0.91. Moreover, the tethered flies were placed in a sealed apparatus such that they did not have any visual cue about the imposed rotation, suggesting that the fly's roll response is mediated by mechanical sensors, consistent with the PI control model.

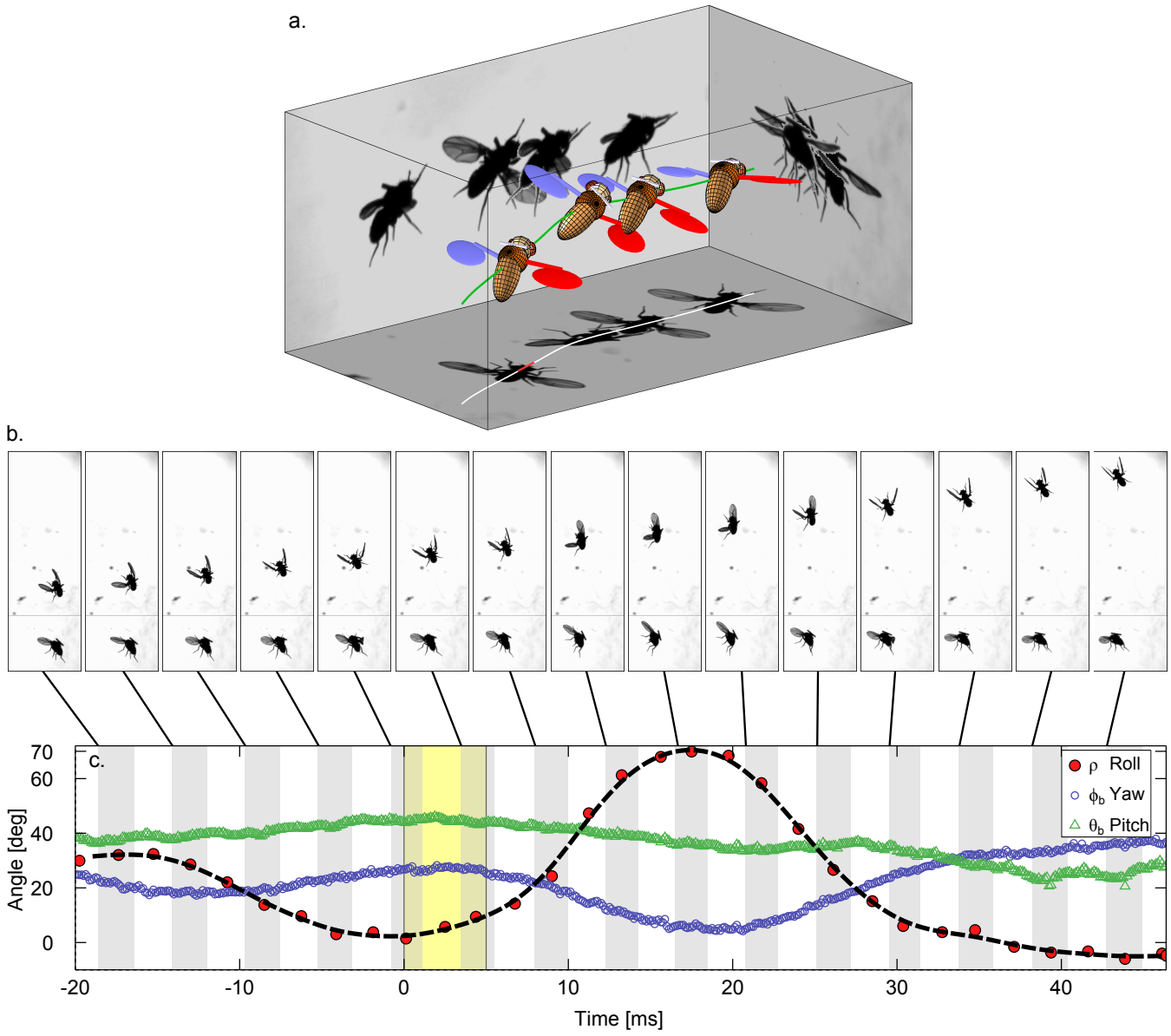

FIG. S.3. Roll perturbation and correction following a double-pulse perturbation. (a) Images from three orthogonal fast cameras of a fruit fly undergoing the perturbation and correction maneuver. Each panel shows 4 superimposed images, before, during and after the second perturbation pulse. The 3D-rendered fly represents the kinematic data of the body and wings. The location of the perturbation (red line) is shown on the fly's center-of-mass trajectory (green line). The second snapshot shows the fly rolled to 70° to its right due to the second perturbation pulse. (b) Top and side-view snapshots of 15 consecutive wing-strokes during the maneuver. Snapshots were taken at the same phase along the wing-stroke, where the wings are in their forward-most position. The snapshots show a clear asymmetry in the wing-stroke amplitude, such that the right wing increased its amplitude and the left wing decreased its amplitude. (c) The body Euler angles during the maneuver. The first perturbation torque was not captured in the movie, but the perturbation of 37° in roll and the recovery are seen in $t = (-20) - 0$ms. The second perturbation torque was on between $0 - 5$ms (yellow stripe), and resulted in a 70° rightward roll deflection. The white and gray stripes represent forward- and back-strokes, respectively. Yaw and pitch angles were sampled at 8000Hz. The roll angle was measured manually in the middle of every half-stroke and smoothed by a quintic spline (black dashed line). Measurement errors are comparable to the size of the plotted symbols.

VI. ADDITIONAL PI CONTROLLER FITS

Figures S.8 - S.10 show three more examples for the fit of the PI controller model. In addition to the fitted curves (red) these plots show that the response of the fly in terms of its wing stroke amplitude asymmetry is continuous, thereby excluding discontinuous control models.

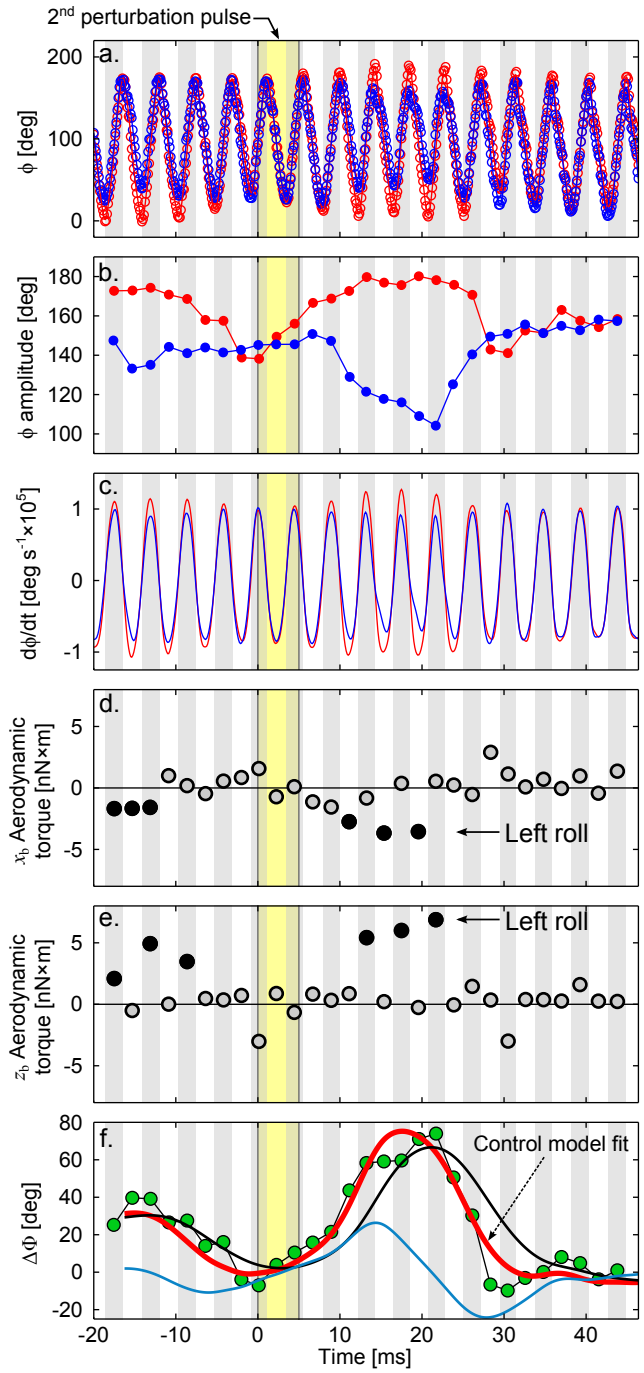

FIG. S.4. Roll correction mechanism for the double-perturbation movie shown in Fig. S1 and Movie 3. (a-c) Wing stroke kinematics as a function of time: (a) The stroke angle ϕ of the right (red) and left (blue) wings; (b) their peak-to-peak amplitude Φ, and (c) their angular velocity $\dot{\phi}$ (c). (d-e) Mean aerodynamic torque along each half stroke, calculated from the measured wing kinematics using a quasi-steady state aerodynamic force model. Solid symbols highlight the correcting wing strokes. (d) the torque component along the body axis $\hat{\mathbf{x}}_\mathrm{b}$, such that negative torque induces a corrective left roll; (e) The torque component along $\hat{\mathbf{z}}_\mathrm{b}$, such that positive values have corrective effect. (f) Wing stroke amplitude difference $\Delta\Phi$ (green), and a fit for a PI controller (eq. 1, red), with $\Delta T = 3.75$ms, $K_\mathrm{p} = 3.5$ms, and $K_\mathrm{i} = 0.95$. The contributions of the 1$^\mathrm{st}$ and 2$^\mathrm{nd}$ terms of Eq. 1 are shown in blue and black, respectively. Measurement errors in (a-f) are comparable to the symbols size.

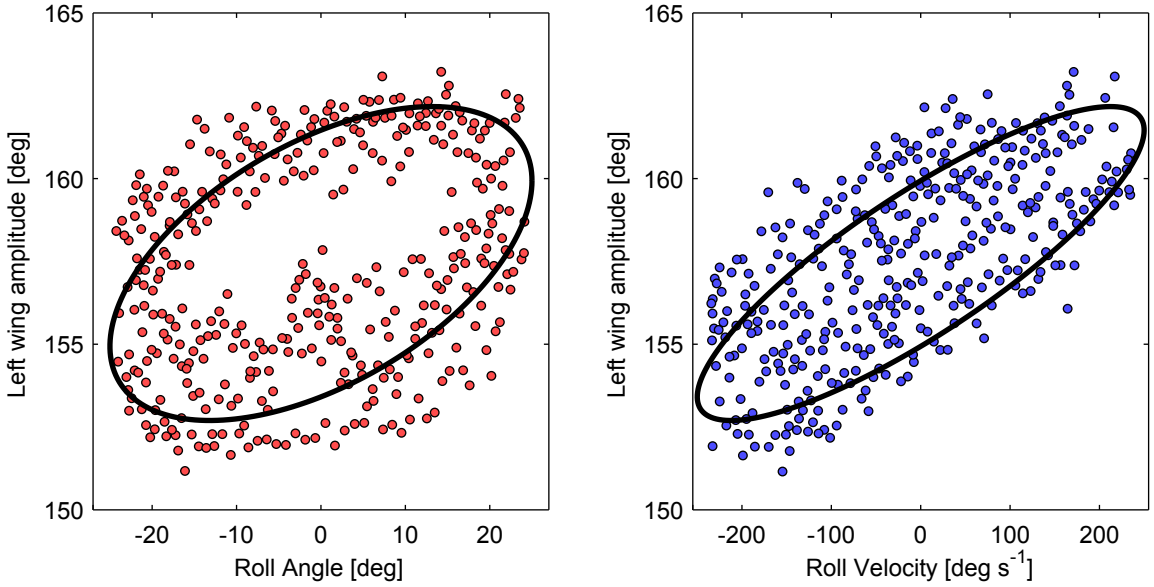

FIG. S.5. The data extracted from [2] for the left wing amplitude in response to a periodic roll oscillation. On the left panel the red circles represent the response to the roll angle. On the right panel the blue circles represent the response to the roll velocity in the same measurement. The black solid ellipses on both panel show the predicted response of a PI control model.

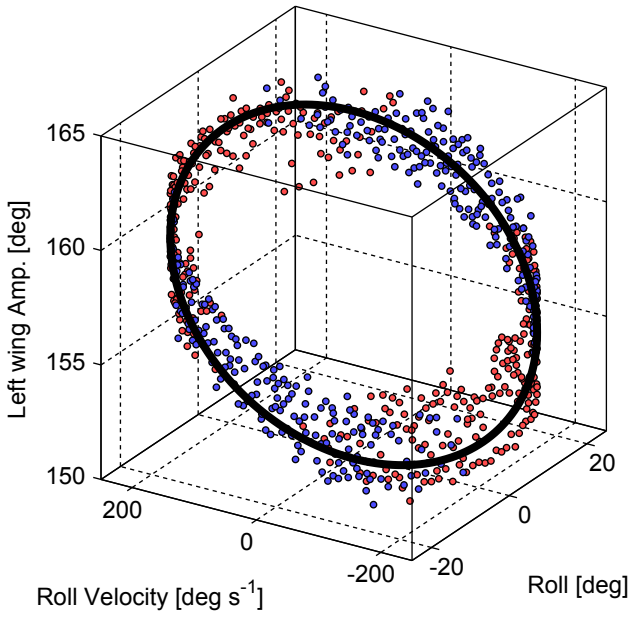

FIG. S.6. The data extracted from [2] for the left wing amplitude in response to a periodic roll oscillation is plotted in the 3D space whose axes are (ρ, $\dot{\rho}$, Φ_{Left}). The data points are colored according to their original color in (Fig. S.5). The black solid line shows the predicted response of the same PI control model shown in Fig. S.5.

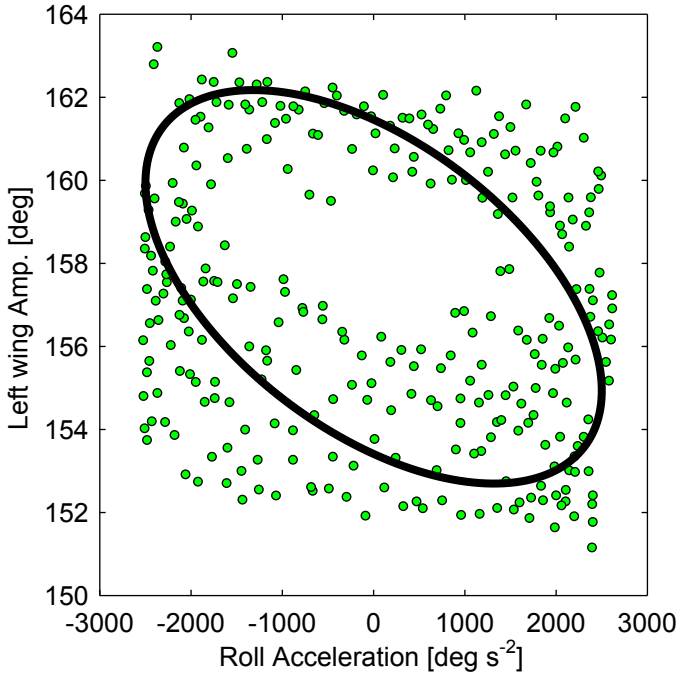

FIG. S.7. The data extracted from [2] for the left wing amplitude in response to a periodic roll oscillation is plotted as a function of roll acceleration. The black solid line shows the predicted response of the same PI control model. Importantly, the PI model is a function of roll angle and roll velocity, and does not include the roll acceleration. The plot shows that the PI model can explain the observed behavior without using the roll acceleration. It supports the hypothesis that fruit flies do not measure their roll acceleration.

[1] L. Ristroph, G. J. Berman, A. J. Bergou, Z. J. Wang, and I. Cohen, Journal of Experimental Biology **212**, 1324 (2009).

[2] M. H. Dickinson, Philosophical Transactions of the Royal Society of London.Series B: Biological Sciences **354**, 903 (1999).

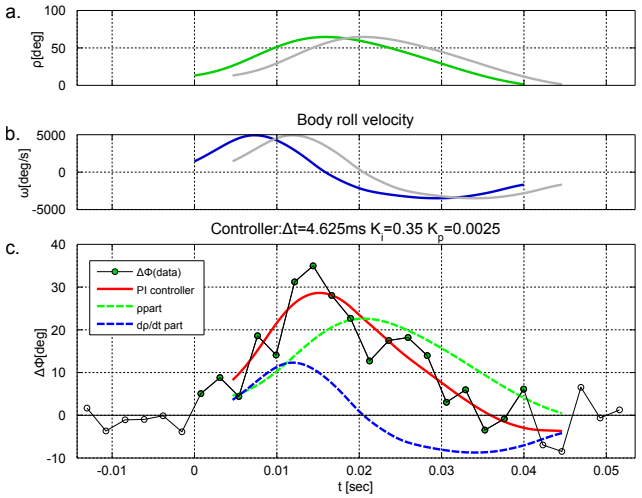

FIG. S.8. PI controller fit. (a) The roll angle ρ as a function of time (green). The gray line is ρ shifted by ΔT, which is the fitted time delay for the PI controller model. (b) The roll velocity $\dot{\rho}$ (blue). The gray line is $\dot{\rho}$ shifted by ΔT. (c) The wing stroke amplitude asymmetry (green circles) $\Delta\Phi$ measured as a function of time for each half stroke. The red line is the response of the fitted PI controller. The dashed green line shows the contribution of the integral term of the controller, namely $K_{\rm i}\rho(t-\Delta T)$. The dashed green line shows the contribution of the proportional term $K_{\rm p}\dot{\rho}(t-\Delta T)$. Both terms have comparable contrubitions to the overall response.

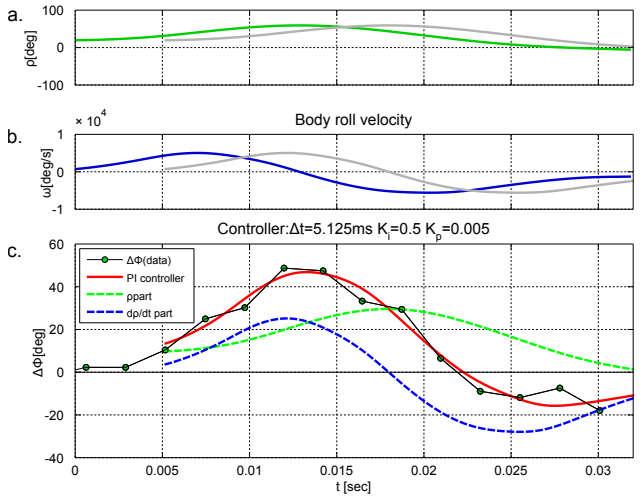

FIG. S.9. Similar plots to the ones in Fig. S.8 for a different correction maneuver.

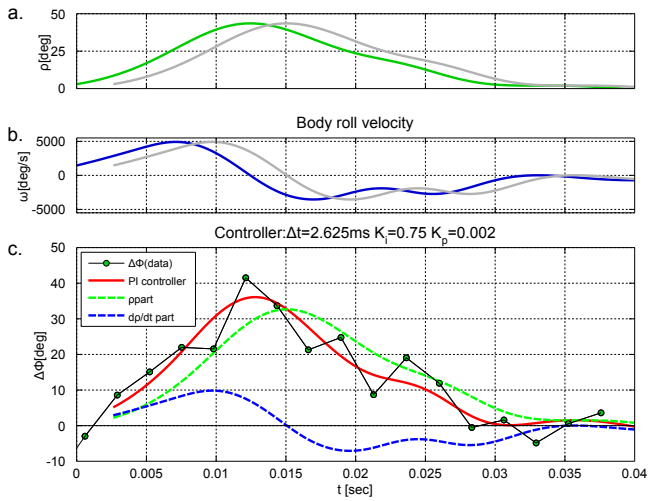

FIG. S.10. Similar plots to the ones in Figs. S.8 and S.9 for a third correction maneuver.